NEAR-ULTRAVIOLET AND NEAR-INFRARED CHARACTERIZATION OF SPACE WEATHERING AT LUNAR MAGNETIC ANOMALIES. David T. Blewett[1], Brett W. Denevi[1], Joshua T.S. Cahill[1], and Rachel L. Klima[1]. [1]Planetary Exploration Group, Johns Hopkins University Applied Physics Laboratory, Laurel, MD 20723, USA (david.blewett@jhuapl.edu).

Introduction: Solar-wind ion bombardment is one of the agents responsible for altering the optical properties of materials that are exposed on the surfaces of airless Solar System bodies. Micrometeoroid impacts are also thought to play an important role in such optical alteration, which is termed "space weathering" (reviewed by [1]), although the relative contribution to space weathering by the solar wind and micrometeoroids is not fully understood and can vary from place to place in the Solar System [e.g., 2]. As studied with reflectance spectroscopy, lunar space weathering involves introduction of a strong positive spectral slope from the visible (vis) to near-infrared (NIR), reduction in the contrast of ferrous iron absorption bands near 1 and 2 μm, and an overall decrease in reflectance. Such optical changes are evident in the differences between the spectrum of a lunar soil and that of a powdered lunar rock of the same composition [e.g., 3, 4]. The optical alteration is caused by the accumulation of submicroscopic blebs and vapor-deposited coatings of metallic iron (SMFe) [5, 1]. Smaller SMFe, with diameters <~30 nm and sometimes called nanophase iron ($npFe^0$) causes darkening and strong reddening [6]. Larger SMFe (>~50 nm) mainly causes darkening [7, 8, 9].

Space Weathering in the UV: Hendrix and Vilas [10] called attention to the effects of lunar-style space weathering in the ultraviolet (UV). At UV wavelengths, surface scattering from regolith grains dominates over volume scattering. Hence, the reflectance in the UV is highly sensitive to vapor-phase SMFe coatings that are produced on regolith particles by space weathering. Global images of the Moon in near UV (NUV) wavelengths collected by the *Lunar Reconnaissance Orbiter* Camera Wide Angle Camera (LROC-WAC) are now available [11, 12], permitting comparisons between the optical properties of fresh and mature materials in the UV, visible, and NIR.

Lunar Samples: In Fig. 1, using laboratory spectra for lunar rocks and soils [13], we show the NUV slope computed between 321 and 415 nm (wavelengths chosen to correspond to LROC-WAC filters). We also calculated the NIR continuum slope across the 1-μm absorption band (B1), by fitting a line to each spectrum at points near 700-750 nm and 1500-1550 nm. We use the B1 continuum slope because we wish to focus on the reddening effects of SMFe. The B1 slope is thus favored over the 950-nm/750-nm reflectance ratio, which is a function of both the continuum slope and the strength of the 1-μm band. Fig. 1 shows the contrast between crushed rock (fresh material with zero exposure to space weathering) and a lunar soil. The soils have steep (red) B1 continua and shallow (blue) NUV slopes. The reverse is true of the rocks, which have shallow B1 continua but steep NUV slopes. A similar plot was presented by [10].

Anomalous Weathering–Lunar Swirls: Areas of magnetized crustal rocks on the Moon, known as magnetic anomalies, were discovered with data from the *Apollo* subsatellite magnetometers [e.g., 14]. Mapped globally by *Lunar Prospector* [e.g., 15, 16], magnetic anomalies are known to affect the ability of solar-wind ions to reach the lunar surface [e.g., 17, 18, 19]. Hence, it might be expected that a magnetically shielded area could experience atypical space weathering [20]. Indeed, the unusual high-albedo markings called lunar swirls [e.g., 21, 22, 23, 24, 25] are all collocated with magnetic anomalies, consistent with the presence of material that is less weathered than that found in mature non-shielded areas.

We have undertaken an analysis of spectral trends associated with swirls in order to gain further insight into the nature and origin of these features. In this contribution, we simultaneously examine swirls in the NUV (LROC-WAC) and NIR (*Chandrayaan* Moon Mineralogy Mapper (M^3)).

Spacecraft Observations: Prior studies have examined lunar swirls at *Clementine* UVVis wavelengths [e.g., 26, 23, 24, 27, 28], and with NIR spectra from Earth-based telescopes [29], the *Clementine* NIR camera [24], and M^3 [30, 31]. LROC NUV images have proven to be extremely useful for mapping swirls [12, 25], and reveal swirl-like patterns that are not readily apparent in the visible.

We follow the analysis of Hemingway et al. [28], who defined regions of interest (ROIs) on and around the high-reflectance portions of swirls in *Clementine* UVVis images in order to characterize the behavior in terms of the 950-nm/750-nm reflectance ratio and 750-nm reflectance. We use corresponding ROIs in M^3 and LROC NUV images (Fig. 2), extracting average spectra and computing the B1 continuum slope at M3 wavelengths 750 and 1549 nm. The NUV slope was calculated from LROC 415- and 321-nm reflectances.

Fig. 3 shows results for the Reiner Gamma swirl. Hemingway et al. found that the swirl maturity trajectory in a plot of 950-nm/750-nm ratio vs. 750-nm reflectance is shallower than the weathering trend seen in areas that are not affected by the presence of a magnetic anomaly. Fig. 3 demonstrates that the normal and anomalous (swirl) trends are evident in the NUV and NIR. Analysis and mapping of these trends will provide key information on the abundance of smaller and larger SMFe in shielded regolith, and the roles of ion and meteoroid bombardment in lunar space weathering.

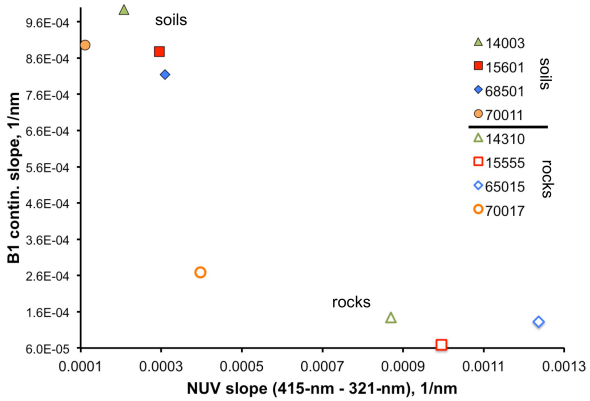

Fig. 1. Plot of B1 continuum slope vs. NUV slope, for spectra of lunar soils and crushed lunar rocks [13, 10]. As material matures, the B1 continuum increases (reddens) while the NUV slope decreases (becomes bluer).

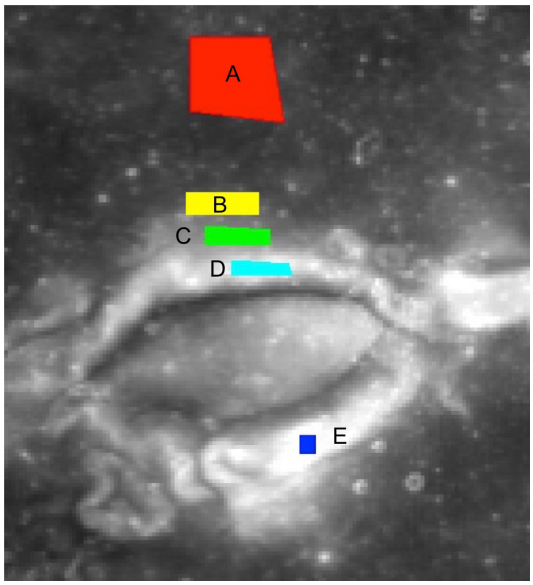

Fig. 2. LROC 415-nm image of the Reiner Gamma swirl, with ROIs. Not shown: ROI for a small fresh crater away from the magnetic and albedo anomaly.

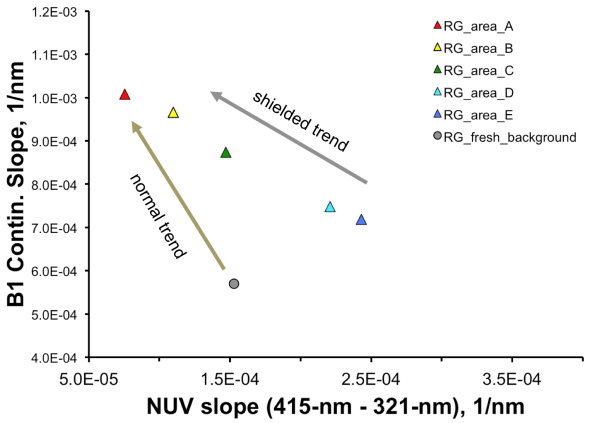

Fig. 3. Plot of B1 continuum slope vs. NUV slope for average spectra extracted from the Reiner Gamma ROIs of Fig. 2. "Area A" represents mature background; "fresh background" is a small fresh crater away from the magnetic and albedo anomaly. The weathering trend within the swirl is shallower than the trend associated with maturation in normal regolith.

References: [1] B. Hapke (2001), *JGR 106*, 10,039–10,073. [2] D. Domingue et al. (2014), *SSR 181*, 121–214. [3] J. Adams and R. Jones (1970), *Science 167*, 737. [4] B. Hapke et al. (1970), *Proc. Apollo 11 LSC*, 2199. [5] C. Pieters et al. (2000), MPS 35, 1101-1107. [6] S. Noble et al. (2007), *Icarus 192*, 629–642. [7] D. Britt and C. Pieters (1994), *GCA 58*, 3905–3919. [8] P. Lucey and S. Noble (2008), *Icarus 197*, 348–353. [9] P. Lucey and M. Riner (2011), *Icarus 212*, 451-462. [10] A. Hendrix and F. Vilas (2006), *Astron. J. 132*, 1396–1404. [11] A. Boyd et al. (2012), *LPSC 43rd*, abstr. 2795. [12] B. Denevi et al. (2014), *JGRP 119*, doi:10.1002/2013JE004527. [13] J. Wagner et al. (1987), *Icarus 69*, 14–28. [14] P. Coleman et al. (1972), *Moon 4*, 419–429. [15] L. Hood et al. (2001), *JGR 106*, 27,825–27,839. [16] J. Halekas et al. (2001), *JGR 106*, 27,841–27,852. [17] M. Kurata et al. (2005), *GRL 32*, L24205. [18] J. Halekas et al. (2008), *PSS 56*, 941–946. [19] M. Weiser et al. (2010), *GRL 37*, L05103. [20] L. Hood and G. Schubert (1980), *Science 208*, 49–51. [21] P. Schultz and L. Srnka (1980), *Nature 284*, 22–26. [22] L. Hood and C. Williams (1989), *Proc. LPSC 19th*, 99–113. [23] D. Blewett et al. (2011), *JGR 116*, E02002. [24] G. Kramer et al. (2011a), *JGR 116*, E04008. [25] B. Denevi et al. (2016), *Icarus*, in press. [26] P. Pinet et al. (2000), *JGR 105*, 9457–9475. [27] I. Garrick-Bethell et al. (2011), *Icarus 212*, 480–492. [28] D. Hemingway et al (2015), *Icarus 261*, 66–79. [29] J. Bell and B. Hawke (1981), *Proc. LPSC 12th*, 679–694. [30] G. Kramer et al. (2011b), *JGR 116*, E00G18. [31] C. Pieters et al. (2014), *LPSC 45th*, abstr. 1408.